Oligosaccharide Preferences of β1,4-Galactosyltransferase-I: Crystal Structures of Met340His Mutant of Human β1,4-Galactosyltransferase-I with a Pentasaccharide and Trisaccharides...

ARTICLE *in* JOURNAL OF MOLECULAR BIOLOGY · NOVEMBER 2005

Impact Factor: 4.33 · DOI: 10.1016/j.jmb.2005.07.050 · Source: PubMed

6 AUTHORS, INCLUDING:

Boopathy Ramakrishnan
Visterra, Inc.
76 PUBLICATIONS **2,030** CITATIONS
SEE PROFILE

Pradman K Qasba
U.S. Department of Health and Human Ser...
123 PUBLICATIONS **2,765** CITATIONS
SEE PROFILE

doi:10.1016/j.jmb.2005.07.050 J. Mol. Biol. (2005) 353, 53–67

JMB

Available online at www.sciencedirect.com

SCIENCE DIRECT®

ELSEVIER

Oligosaccharide Preferences of β1,4-Galactosyltransferase-I: Crystal Structures of Met340His Mutant of Human β1,4-Galactosyltransferase-I with a Pentasaccharide and Trisaccharides of the *N*-Glycan Moiety

Velavan Ramasamy[1], Boopathy Ramakrishnan[1,2] Elizabeth Boeggeman[1,2], Daniel M. Ratner[3], Peter H. Seeberger[3,4] and Pradman K. Qasba[1]*

[1]*Structural Glycobiology Section, Laboratory of Experimental and Computational Biology, Center for Cancer Research, National Cancer Institute at Frederick Frederick, MD 21702, USA*

[2]*Basic Research Program SAIC-Frederick, Inc.; Laboratory of Experimental and Computational Biology, Center for Cancer Research, National Cancer Institute at Frederick Frederick, MD 21702, USA*

[3]*Department of Chemistry Massachusetts Institute of Technology, Cambridge, MA 02139, USA*

[4]*Laboratorium für Organische Chemie, ETH Hönggerberg/HCI F 315, Wolfgang-Pauli-Strasse 10, CH-8093, Zürich Switzerland*

**Corresponding author*

β-1,4-Galactosyltransferase-I (β4Gal-T1) transfers galactose from UDP-galactose to *N*-acetylglucosamine (GlcNAc) residues of the branched *N*-linked oligosaccharide chains of glycoproteins. In an *N*-linked biantennary oligosaccharide chain, one antenna is attached to the 3-hydroxyl-(1,3-arm), and the other to the 6-hydroxyl-(1,6-arm) group of mannose, which is β-1,4-linked to an *N*-linked chitobiose, attached to the aspargine residue of a protein. For a better understanding of the branch specificity of β4Gal-T1 towards the GlcNAc residues of *N*-glycans, we have carried out kinetic and crystallographic studies with the wild-type human β4Gal-T1 (h-β4Gal-T1) and the mutant Met340His-β4Gal-T1 (h-M340H-β4Gal-T1) in complex with a GlcNAc-containing pentasaccharide and several GlcNAc-containing trisaccharides present in *N*-glycans. The oligosaccharides used were: pentasaccharide GlcNAcβ1,2-Manα1,6 (GlcNAcβ1,2-Manα1,3)Man; the 1,6-arm trisaccharide, GlcNAcβ1,2-Manα1,6-Manβ-OR (1,2-1,6-arm); the 1,3-arm trisaccharides, GlcNAcβ1,2-Manα1,3-Manβ-OR (1,2-1,3-arm) and GlcNAcβ1,4-Manα1,3-Manβ-OR (1,4-1,3-arm); and the trisaccharide GlcNAcβ1,4-GlcNAcβ1,4-GlcNAc (chitotriose). With the wild-type h-β4Gal-T1, the K_m of 1,2-1,6-arm is approximately tenfold lower than for 1,2-1,3-arm and 1,4-1,3-arm, and 22-fold lower than for chitotriose. Crystal structures of h-M340H-β4Gal-T1 in complex with the pentasaccharide and various trisaccharides at 1.9–2.0 Å resolution showed that β4Gal-T1 is in a closed conformation with the oligosaccharide bound to the enzyme, and the 1,2-1,6-arm trisaccharide makes the maximum number of interactions with the enzyme, which is in concurrence with the lowest K_m for the trisaccharide. Present studies suggest that β4Gal-T1 interacts preferentially with the 1,2-1,6-arm trisaccharide rather than with the 1,2-1,3-arm or 1,4-1,3-arm of a bi- or tri-antennary oligosaccharide chain of *N*-glycan.

Published by Elsevier Ltd.

Keywords: β-1,4-galactosyltransferase-I; conformational change; *N*-glycan trisaccharides; human-β4Gal-T1-oligosaccharide crystal structures; β4Gal-T1 oligosaccharide preferences

Abbreviations used: ER, endoplasmic reticulum; GT, glycosyltransferase; β4Gal-T, β1,4galactosyltransferase; β4Gal-T1, β1,4-Galactosyltransferase-I; b-β4Gal-T1, bovine β4Gal-T1; h-β4Gal-T1, human β4Gal-T1; UDP-Gal, UDP-α-galactose; UDP-H, UDP-hexanolamine; GlcNAc, *N*-acetylglucosamine; GlcNAc-T, *N*-acetylglucosaminyltransferase; OR, $-O\text{-}CH_2\text{-}CH_2\text{-}CH_2\text{-}CH{=}CH_2$; PDB, RCSB protein data base.

E-mail address of the corresponding author:qasba@helix.nih.gov

0022-2836/$ - see front matter Published by Elsevier Ltd.

Introduction

Glycosylation of proteins is the most common biological event in the cell, in which protein function is modulated, leading to a diverse range of cellular functions.[1] *N* and *O*-linked glycosylation are the two most prevalent forms of protein glycosylation found in eukaryotes. *N*-linked glycosylation is the covalent linkage between the oligosaccharides and the amide group of asparagyl residues in proteins resulting in an *N*-linked glycan (*N*-glycan). In contrast, *O*-linked glycosylation is between the sugar and the hydroxyl group of Ser/Thr. The *N*-glycan structures on a protein in the endoplasmic reticulum (ER) are rich in mannose sugars, which undergo extensive modification in the Golgi complex.[2] Complex polymeric-branched matured *N*-glycans (Figure 1) are generated in the Golgi apparatus.[3] The metamorphosis of *N*-glycans is dictated by various glycosyltransferases (GT), a superfamily of enzymes present in both ER and the Golgi complex.

The GT superfamily is classified into families, depending upon the transfer of specific monosaccharides from sugar donors to the various acceptors.[4] Each GT family is responsible for a particular donor-acceptor linkage in which the anomeric configuration of the transferred donor is either retained (α) or inverted (β), leading to the expansion of a particular family into subfamilies. The galactosyltransferase (Gal-T) family transfers galactose from UDP-galactose to various acceptor substrates through β1-4, β1-3, α1-3, and α1-4 linkages. Seven members in the β1,4-galactosyltransferase (β4Gal-T) subfamily, T1 to T7, are known to date,[5] and all use UDP-α-galactose (UDP-Gal) as the donor substrate. However, each member has a sequence variation at the acceptor-binding site,[6] thereby displaying unique acceptor specificity.[7]

β1,4-Galactosyltransferase-I (β4Gal-T1) is a classic example of a type-II membrane protein with a cytoplasmic domain, transmembrane domain, a stem region, and a globular catalytic domain facing the Golgi lumen.[8] The length and amino acid composition are well conserved in the catalytic domain, but variation in protein sizes among family members is contributed from the stem region.[5] The β4Gal-T1 transfers galactose from UDP-Gal to a monosaccharide acceptor *N*-acetylglucosamine (GlcNAc), or to the non-reducing end GlcNAc of the complex *N*-glycan structure (Figure 1). The acceptor specificity of β4Gal-T1 is altered from GlcNAc to glucose by α-lactalbumin (a modifier protein), resulting in the production of lactose,[9] which is secreted in milk.

Bovine β4Gal-T1 (b-β4Gal-T1) is the first mammalian GT whose three-dimensional structure of the catalytic domain was determined without substrate in an open conformation,[10] and with substrate in a closed conformation.[11] The sugar nucleotide donor and cofactor Mn^{2+}-bound structure shows large conformational changes in the enzyme compared to the unbound structure, in that a long loop (I345-H365) and a short loop (G313-G316) in b-β4Gal-T1 (corresponding residues, I341-H361 and G309-G312, in human β4Gal-T1 (h-β4Gal-T1)) move towards the catalytic pocket. The conformational changes create an acceptor-binding site for GlcNAc or GlcNAc at the non-reducing end of an *N*-glycan.[6] In the closed conformation, Mn^{2+} has six coordinations, two of which are with α and β-phosphate oxygen atoms of UDP-Gal, three with protein residues His347, Asp254, and Met344 (corresponding residues in h-β4Gal-T1 are His343, Asp250 and Met340), and one with the conserved water molecule.[12] His347 and Asp254 form a stronger coordination bond with Mn^{2+} than with Met344. The mutation of the

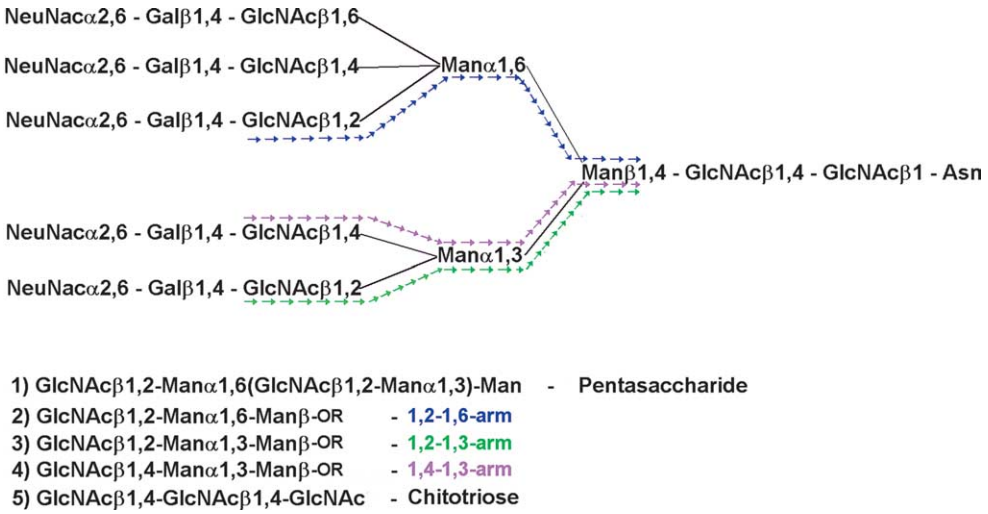

Figure 1. A depiction of complex penta-antennary *N*-glycan structure. The pentasaccharide and the trisaccharides of the *N*-glycan moiety, used for the kinetic and crystallographic studies, are highlighted by colored arrows. GlcNAcβ1,2-Manα1,6(GlcNAcβ1,2-Manα1,3)-Man pentasaccharide (blue and green arrows); GlcNAcβ1,2-Manα1,6-Manβ-OR (1,2-1,6-arm) (blue arrows); GlcNAcβ1,2-Manα1,3-Manβ-OR (1,2-1,3-arm) (green arrows); GlcNAcβ1,4-Man α1,3-Manβ-OR (1,4-1,3-arm) (purple arrows).

residues His347 and Asp254 results in the loss of enzymatic activity.[13]

In an earlier study, we showed that when the metal-coordinating residue Met344 of b-β4Gal-T1 is mutated to His, the mutant b-M344H-Gal-T1 loses 98% of its Mn^{2+}-dependent enzyme activity compared to the wild-type b-β4Gal-T1, but is activated in the presence of Mg^{2+}.[14] The metal ion Mn^{2+} binds tightly to b-M344H-β4Gal-T1 in the presence of UDP-hexanolamine (UDP-H), and the mutant enzyme readily changes to the closed conformation, creating the oligosaccharide acceptor-binding site.[14] The mutant b-M344H-β4Gal-T1, in the presence of Mn^{2+} and UDP-H, could be crystallized with different oligosaccharide acceptors, thus allowing the analysis of the oligosaccharide binding site, whereas the enzyme activity of the mutant could be measured in the presence of Mg^{2+}.

In the present study, our aim was to find out the specificity of β4Gal-T1 towards the oligosaccharides of the arms of a biantennary *N*-glycan. The kinetic investigations of the wild-type h-β4Gal-T1 in the presence of Mn^{2+}, or h-M340H-β4Gal-T1 mutant in the presence of Mg^{2+}, with various oligosaccharides of *N*-glycan moiety show that the 1,2-1,6-arm trisaccharide at low concentrations is a preferred acceptor substrate for the enzyme, while at higher concentrations, the trisaccharide shows substrate inhibition. The bovine mutant b-M344H-β4Gal-T1, which gave crystals with a disaccharide chitobiose,[14] failed to give crystals in complex with *N*-glycans or their fragments. In contrast, the human mutant h-M340H-β4Gal-T1 gave crystals in complex with a pentasaccharide, and four different trisaccharides of the *N*-glycan moiety, and their crystal structures are described here. The structural studies suggest also that the trisaccharide of the 1,2-1,6-arm makes the maximum number of interactions with β4Gal-T1.

Results and Discussion

Upon substrate binding, β4Gal-T1 undergoes conformational changes from an open to closed conformation.[6,11] The acceptor-binding site of b-β4Gal-T1 is created in the closed conformation, where Tyr286 and Phe280 (corresponding residues, Tyr282 and Phe276 in h-β4Gal-T1) are accessible for the binding of GlcNAc or the binding of branched oligosaccharide chains.[6] In our earlier study with b-β4Gal-T1, we mutated the weak metal-coordinating residue Met344 to His to strengthen the primary metal-binding site, which favors the closed conformation of the enzyme in the presence of Mn^{2+} or Mg^{2+}, and UDP-H or UDP-Gal.[14] The acceptor-binding site exists only in the closed conformation. To delineate the acceptor-binding site of the enzyme and the specificity towards various oligosaccharides that represent the arms of the *N*-linked biantennary oligosaccharide chain, we have carried out enzyme kinetic analysis with the wild-type h-β4Gal-T1, using a pentasaccharide and different oligosaccharides as acceptors, and determined the crystal structures of the h-M340H-β4Gal-T1 mutant in complex with these oligosaccharides.

Kinetic parameters of the oligosaccharide acceptor substrates for h-β4Gal-T1

Using a variety of trisaccharides, some corresponding to structures found in the branched *N*-linked oligosaccharides, we determined the branch specificity of h-β4Gal-T1. The double substrate kinetic data for the enzyme in the presence of chitobiose or chitotriose fit best to a rate equation that lacks k_{ia}, the dissociation constant of the UDP-Gal-metal-enzyme complex, suggesting that the donor substrate does not dissociate from the enzyme–substrate complex. The true K_m for both chitobiose and chitotriose is nearly the same (Table 1), suggesting that the presence of an additional GlcNAc residue in chitotriose, which does not appear in chitobiose, does not affect the ground-state binding of these acceptor substrates to the enzyme. Moreover, the apparent K_m value for chitobiose and chitotriose, determined at a fixed concentration of UDP-Gal and various concentrations of acceptor, is similar to the true K_m value obtained by double-substrate kinetics.

Due to the limited quantities of the synthetic trisaccharides of 1,2-1,6-, 1,2-1,3-, and 1,4-1,3-arms, a double-substrate kinetic analysis could not be performed. Instead, the apparent K_m was determined

Table 1. Kinetic parameters of the mono-, di- and oligosaccharide acceptors

Sugar acceptors	True K_m (mM)	Apparent K_m (mM)	V_{max} (pmol min^{-1} ng^{-1})	k_{cat} (s^{-1})	k_{cat}/K_m (s^{-1} mM^{-1})
GlcNAc	10(1)	ND	6.4(4)	3.6	0.3
GlcNAcβ1,4-GlcNAc	1.51(1)	1.59(32)	8.45(25)	4.82	3.19
Chitotriose[a]	1.51(1)	0.96(14)	8.44(14)	4.81	3.18
GlcNAcβ1,2-Man	ND	3.83(40)	7.91(20)	4.48	1.16
GlcNAcβ1,2-Manα1,3-Manβ-OR	ND	0.60(15)	4.36(10)	2.47	4.09
GlcNAcβ1,4-Manα1,3-Manβ-OR	ND	0.71(16)	5.91(8)	3.35	4.69
GlcNAcβ1,2-Manα1,6-Manβ-OR	ND	0.06(1)	3.35(5)	1.90	31.66
Pentasaccharide[b]	ND	1.23(4)	3.07(3)	1.74	1.41

Standard deviations are given in the parentheses to their least significant decimal point.
[a] GlcNAcβ1,4-GlcNAcβ1,4-GlcNAc.
[b] GlcNAcβ1,2-Manα1,6(GlcNAcβ1,2-Manα1,3)Man.

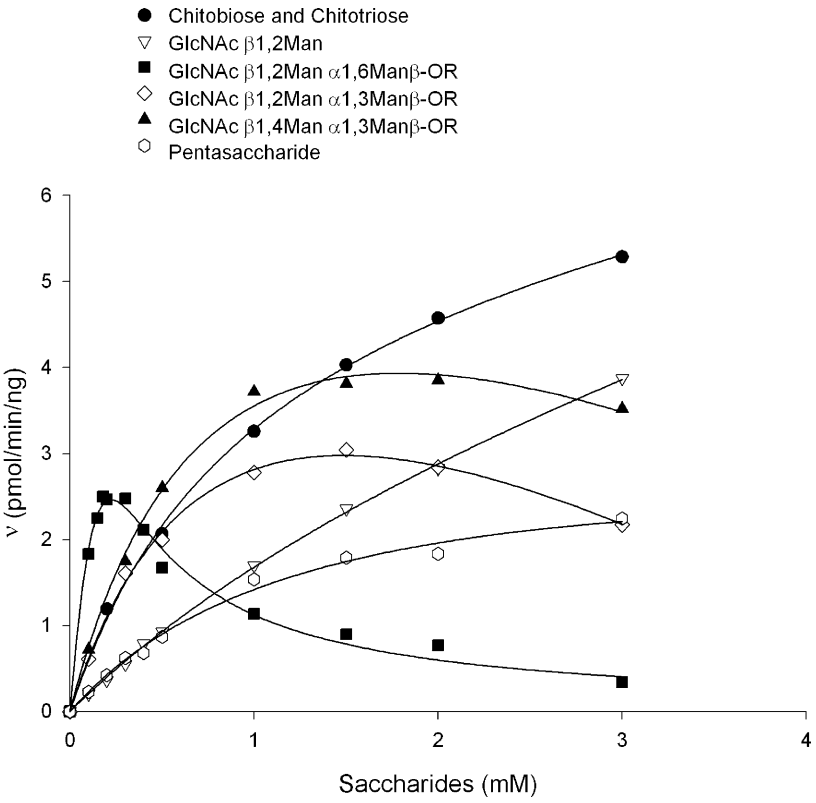

Figure 2. Effects of varying the oligosaccharide acceptor substrate concentration on the initial rate of galactose transfer (v) by the h-β4Gal-T1. Chitobiose (GlcNAcβ1,4-GlcNAc) and chitotriose GlcNAcβ1,4-GlcNAcβ1,4-GlcNAc (●), GlcNAcβ1,2-Man (▽), GlcNAcβ1,2-Manα1,6-Manβ-OR (■), GlcNAcβ1,2-Manα1,3-Manβ-OR (◇), GlcNAcβ1,4-Manα1,3-Manβ-OR (▲), pentasaccharide GlcNAcβ1,2-Manα1,6(GlcNAcβ1,2-Manα1,3)Man(⬡).

for each of the trisaccharide acceptors at fixed concentrations of UDP-Gal and Mn^{2+} (Figure 2; Table 1). The apparent K_m for the trisaccharide GlcNAcβ1,2-Manα1,6-Manβ-OR is approximately tenfold lower than the apparent K_m for both GlcNAcβ1,2-Manα1,3-Manβ-OR and GlcNAcβ1,4-Manα1,3-Manβ-OR. Although there is a slight reduction in the turnover number, k_{cat}, the catalytic efficiency (k_{cat}/K_m) of the enzyme with the acceptor substrate GlcNAcβ1,2-Manα1,6-Manβ-OR is about eightfold greater than the catalytic efficiency of the enzyme with the acceptors having the Manα1,3-Man disaccharide unit. This difference is due to a decrease in their ground-state binding (K_m), compared to the oligosaccharide containing the Manα1,6-Man disaccharide unit. When compared with the disaccharide GlcNAcβ1,2-Man, the K_m of the trisaccharide GlcNAcβ1,2-Manα1,6-Manβ-OR is 63-fold lower and the catalytic efficiency of the enzyme (k_{cat}/K_m) is 27-fold higher (Table 1). The large decrease in K_m and the minor reduction in k_{cat} indicate that the α1,6-Man residue is undergoing additional interactions (see the crystal structure of the complex with 1,2-1,6-arm), thereby increasing the stability of the ground-state binding with a minor effect on the transition-state complex. The K_m for GlcNAcβ1,2Manα1,6-Manβ-OR is 27-fold and 16-fold lower than that of chitobiose and chitotriose, respectively. Although the k_{cat} decreased by only twofold, the catalytic efficiency increased by tenfold. Thus, with the trisaccharide GlcNAcβ1,2-Manα1,6-Manβ-OR, there is a preferential stabilization of the ground-state Michaelis complex over the stabilization of the transition state.

Effect of the trisaccharide concentrations on the catalytic activity of β4Gal-T1

The acceptor trisaccharide GlcNAcβ1,2-Manα1,6-Manβ-OR shows substrate inhibition at concentrations that are lower by a factor of 10 than those found for the acceptors containing the Manα1,3-Man disaccharide unit linked to GlcNAc at the non-reducing end (Figure 2; Table 1). In a previous study, we showed that the catalytic activity of β4Gal-T1 is inhibited at much higher concentrations of GlcNAc (20–25 mM),[14] and chitobiose and chitotriose do not inhibit the catalytic activity of β4Gal-T1 at the concentrations used in the assay (Figure 2). The GlcNAcβ1,2-Manα1,6-Manβ-OR acceptor has higher affinity for the wild-type enzyme, resulting in a substrate inhibition at concentrations that are much lower than other acceptor substrates. This is consistent with a tenfold to 60-fold reduction in the K_m for GlcNAcβ1,2-Manα1,6-Manβ-OR acceptor, compared to other oligosaccharides used. The catalytic efficiency (k_{cat}/K_m) of the enzyme with respect to the acceptor GlcNAcβ1,2-Manα1,6-Manβ-OR also increased sevenfold compared to GlcNAcβ1,2-Manα1,3-Manβ-OR and GlcNAcβ1,4-Manα1,3-Manβ-OR and almost 100-fold compared to GlcNAc. Thus, our study shows that GlcNAcβ1,2-Manα1,6-Manβ-OR is a preferred acceptor for

β4Gal-T1 at low concentrations, but at higher concentrations, forms a dead-end complex.

Crystal structures of h-M340H-β4Gal-T1–oligosaccharide complexes

The crystal structures of all five of the h-M340H-β4Gal-T1–oligosaccharide complexes possess three molecules/asymmetric unit that are related by an approximate 3-fold non-crystallographic symmetry (angles of 117°, 119°, and 119°). Since we had a sufficient number of reflections-to-parameter ratios, we did not apply NCS during refinement and preferred to treat the three molecules as separate entities (Table 2). The overall structure of all five complexes shows that, in each structure, h-M340H-β4Gal-T1 is in the closed conformation (Figure 3), resembling the closed conformation of b-β4Gal-T1 in the presence of substrates (RCSB protein data base (PDB) code 1O0R).[6] The overall rms deviation of the main-chain atoms between the closed conformation of wild-type b-β4Gal-T1 and h-M340H-β4Gal-T1 in complex with pentasaccharide and trisaccharides (1,2-1,6-arm, or 1,2-1,3-arm or 1,4-1,3-arm or chitotriose) varies between 0.3 Å and 0.4 Å for molecules A, B, and C, indicating that there are no significant structural changes in the overall structure of each molecule. The structures reveal the presence of UDP-H and Mn^{2+} at the same sites as observed in the b-M344H-β4Gal-T1 complexed with UDP-H and chitobiose (PDB code 1TW5),[14] and the wild-type b-β4Gal-T1 complexed with UDP-Gal and Mn^{2+} (PDB code 1O0R).[6] The GlcNAc at the non-reducing end of the oligosaccharides occupies the same position as the GlcNAc monosaccharide in the crystal structure of lactose synthase complexed with GlcNAc[11] (PDB code 1NMM), where GlcNAc makes only five conserved hydrogen bonds with the protein atoms. Their distances are <3.2 Å, and the interactions are as follows: 312 N···O3 of GlcNAc, 355 N^{ε}···O7 carbonyl oxygen atom of GlcNAc, 315 $O^{\delta 2}$···N2 of the *N*-acetyl group in GlcNAc, 314 $O^{\delta 1}$···O3 of GlcNAc, and 314 $O^{\delta 2}$···O4 of GlcNAc. The second and the third saccharides of all five of the complexes are stabilized by hydrophobic interactions with the protein atoms rather than by hydrogen bonds, except that the reducing end GlcNAc of chitotriose is stabilized due to the linearity of the β1,4 linkage.

Crystal structure of h-M340H-β4Gal-T1–pentasaccharide complex

Initially, the human M340H-β4Gal-T1 was co-crystallized with a biantennary heptasaccharide *N*-glycan, Arg-[GlcNAcβ1,2-Manα1,6-(GlcNAcβ1,2-Manα1,3)-Manβ1,4-GlcNAcβ1,4-GlcNAcβ]-Asn-Glu-Gly. The crystals diffracted to a resolution of 2.3 Å. We were unable to see the *N*-glycan in the acceptor-binding site, which was filled with completely diffused partial electron density. Next, we co-crystallized h-M340H-β4Gal-T1 with a pentasaccharide, GlcNAcβ1,2-Manα1,6(GlcNAcβ1,2-Manα1,3) Man, part of a biantennary *N*-glycan carrying both the 1,2-1,6-arm and the 1,2-1,3-arm linked to core mannose. The crystals diffracted X-rays to a resolution of 2.0 Å, and the data showed clear electron density only for the disaccharide unit GlcNAcβ1,2-Man of the bound pentasaccharide (Figure 3(a)). We observed only a partial electron density for the third

Table 2. Data collection and refinement statistics of human M340H-β4Gal-T1 with UDP-H, Mn^{2+} and oligosaccharides

Parameter	Pentasaccharide	1,2-1,6-arm	1,2-1,3-arm	1,4-1,3-arm	Chitotriose
No. reflections	495,491	561,935	556,859	726,977	369,585
No. unique reflections	101,444	100,723	97,860	118,434	102,154
Completeness (%)	96.5	99.6	97.6	100.0	99.9
Resolution range (Å)	50.0–2.0	40.0–2.0	40.0–2.0	40.0–1.9	40.0–2.0
R_{sym}[a]	0.094(0.59)	0.064(0.472)	0.058(0.447)	0.063(0.468)	0.059(0.322)
$<I/\sigma(I)>$	15.0(2.2)	26.6(3.8)	27.2(3.5)	28.3(3.4)	21.1(3.7)
Unit cell dimensions					
a (Å)	107.0	107.2	107.2	107.5	107.5
b (Å)	195.2	195.0	193.0	194.8	195.4
c (Å)	143.9	143.7	143.4	143.7	144.0
R-factor/R_{free}	0.219/0.246	0.208/0.239	0.204/0.232	0.202/0.228	0.202/0.224
No. reflections used in refinement	97,969	100,651	97,670	118,247	101,948
No. protein atoms	6636	6636	6636	6654	6636
No. ligand atoms/Mn^{2+}	185/3	207/3	207/3	207/3	225/3
No. water molecules	471	488	424	532	548
Glycerol/SO_4^{2-}/dioxane molecules	7/14/1	7/14/1	8/13/1	8/16/1	7/16/2
Coordinate error (Luzzati plot, cross-validated)	0.30	0.29	0.28	0.26	0.27
rms deviations from ideal					
Bond lengths (Å)	0.009	0.010	0.010	0.010	0.011
Bond angles (deg.)	1.55	1.53	1.52	1.51	1.54
Dihedrals (deg.)	24.25	24.12	23.98	24.01	24.07
Improper (deg.)	1.00	1.00	1.00	1.00	1.03
Ramachandran plot statistics					
Most favored regions (%)	88.3	89.0	88.6	88.8	89.7
Additionally allowed regions (%)	11.7	11.0	11.4	11.2	10.3

[a] Values in parentheses are for the outermost shell.

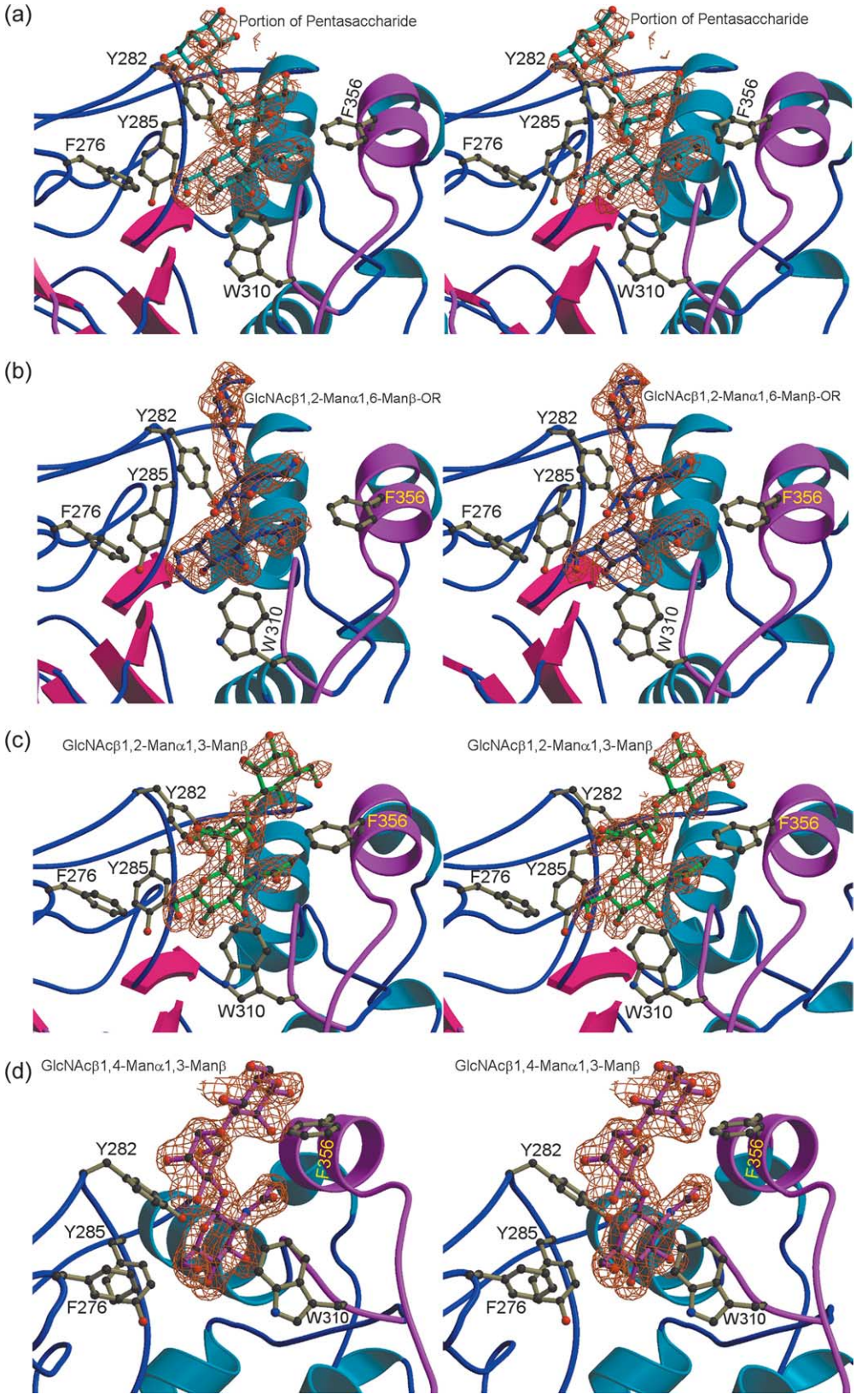

Figure 3 (*legend next page*)

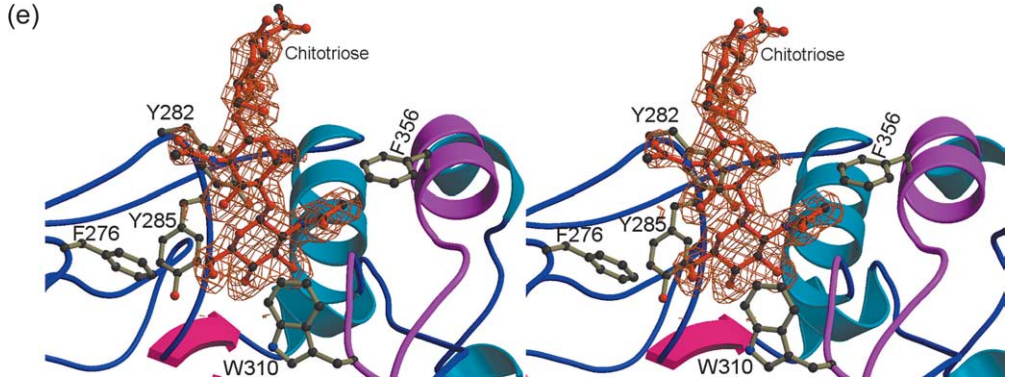

Figure 3. Stereo view of the difference Fourier electron density omit maps contoured at the 2.0σ level around (a) a portion of the visible pentasaccharide, and at the 2.5σ level around four different trisaccharides: (b) 1,2-1,6-arm; (c) 1,2-1,3-arm; (d) 1,4-1,3-arm; and (e) chitotriose. Displayed are the key residues of h-β4Gal-T1, F276, Y282, Y285, W310, and F356, which are involved in the hydrophobic interactions. The linker (-OR), which is attached to the mannose at the reducing end of the synthetic trisaccharide, is not visible.

residue contoured at the 2.0σ level, which fit best to α1,6 linked Man (core mannose) with 70% occupancy.

The glycosidic dihedral angles of the β1,2-linkage, the ϕ, ψ values (refer to Table 3 for the nomenclature of ϕ, ψ angles) in the bound pentasaccharide, are comparable with the values found in the β1,2-linkage observed in the crystal structure of the complex with the trisaccharide GlcNAcβ1,2-Manα1,6-Manβ-OR (1,2-1,6-arm) (described below) (Table 3). However, these ϕ, ψ values of β1,2-linkage differ drastically from the ϕ, ψ values of the β1,2-linkage in the complex with the GlcNAcβ1,2-Manα1,3-Manβ-OR (1,2-1,3-arm) trisaccharide. Even though we were able to see only the partial structure of the pentasaccharide with partial occupancy for the core mannose molecule (middle mannose), there were 13 interactions between the protein atoms and the pentasaccharide, fewer than the number found in the 1,2-1,6-arm trisaccharide complex (Table 4A).

In about 50% of the carbohydrate–protein crystal structures in the PDB, only part of the glycan was seen in the electron density maps, suggesting a high degree of glycan mobility or spatial disorder. The crystal structure of h-M340H-β4Gal-T1 in complex with the pentasaccharide also shows disordered sugar units due to the flexibility of the glycan moiety. Since the crystal packing hinders the binding of heptasaccharide, and only a trisaccharide portion of the pentasaccharide can be located in the complex, we investigated further the crystal structures of the complexes of h-M340H-β4Gal-T1 with only the trisaccharides of the *N*-glycan moiety.

Crystal structures of h-M340H-β4Gal-T1–trisaccharides complexes

Structure of the complex with the GlcNAcβ1,2-Manα1,6-Manβ-OR (1,2-1,6-arm) trisaccharide

Complete and clear electron density was observed for the 1,2-1,6-arm trisaccharide bound to h-M340H-β4Gal-T1. The mannose residue at the reducing end (core mannose) that is linked to the mannose in the middle *via* α1-6-linkage makes hydrophobic interactions with Tyr282 (Figure 3(b)). Since α1,6-linkage possesses, in addition to ϕ and ψ dihedral angles, one additional conformational degree of freedom, ω (Table 3), it has more flexibility to make the best possible contacts with the protein atoms. While α1,6-linked reducing end mannose interacts with the protein atoms, the middle mannose acts as a hinge. The Manα1,6-Man linkage is less restrained than any of the other linkages, adopting a wide range of conformational space rather than a well-defined unique conformation.[15] Thus, the dihedral angles of the Manα1,6-Man linkage have deviated from the mean values observed in 145 crystal structures.[16,17] The dihedral angles of the GlcNAcβ1,2-Man linkage ($\phi = -87.5(\pm 3.4)°$ and $\psi = -84(\pm 10.9)°$) in 1,2-1,6-arm are in agreement with the 53 crystal structures of the protein–carbohydrate complexes containing this linkage.[16,17] The 1,2-1,6-arm dihedral angles are given in Table 3. Figure 3(b) shows the stereo view diagram of the difference Fourier electron density omit maps contoured at the 2.5σ level around the 1,2-1,6-arm, and the key residues F276, Y282, Y285, W310, and F356, which are involved in hydrophobic interactions, are displayed. The 1,2-1,6-arm is stabilized in this complex by a maximum number of hydrophobic interactions between the ligand and the protein atoms, compared to the other three trisaccharide complexes (Table 4A).

Structure of the complex with GlcNAcβ1,2-Manα1,3-Manβ-OR (1,2-1,3-arm) trisaccharide

The observed electron density for the 1,2-1,3-arm is clear for the non-reducing end GlcNAc and the second residue, β1,2 linked mannose (middle Man), whereas the third residue, the reducing end α1-3-Man, has a partial occupancy (70%) for the two molecules in the asymmetric unit (Figure 3(c)). The dihedral angles observed for GlcNAcβ1,2-Man linkage ($\phi = -107.2(\pm 1.5)°$ and $\psi = -128.0$

Table 3. Dihedral angles (deg.) of partially visible pentasaccharide and trisaccharides bound with human M340H-β4Gal-T1

	Visible portion of pentasaccharide GlcNAcβ1,2-Manα1,6-Man					1,2-1,6-arm GlcNAcβ1,2-Manα1,6-Manβ-OR					1,2-1,3-arm GlcNAcβ1,2-Manα1,3-Manβ-OR			
	Gnβ1,2-Mn		Mnα1,6-Mnβ			Gnβ1,2-Mn		Mnα1,6-Mnβ			Gnβ1,2-Mn		Mnα1,3-Mnβ	
Monomer	ϕ_1	ψ_1	ϕ_2	ψ_2	ω_2	ϕ_1	ψ_1	ϕ_2	ψ_2	ω_2	ϕ_1	ψ_1	ϕ_2	ψ_2
A	−61.3	−82.5	–	–	–	−85.9	−71.7	79.2	172.1	159.7	−108.9	−127.4	62.0	−141.9
B	−60.8	−81.3	77.3	−179.8	82.6	−85.3	−90.2	105.3	179.1	151.7	−105.9	−127.6	60.9	−144.7
C	−59.8	−99.9	–	–	–	−91.4	−90.9	122.6	170.8	139.5	−106.9	−129.1	63.4	−136.0
Average	−60.3	−87.9				−87.5	−84.3	102.4	174.2	150.5	−107.2	−128.0	62.1	−141.0
S.D	0.8	10.4				3.4	10.9	21.9	4.4	10.9	1.5	0.9	1.3	4.4
SWEET (Model)	−97.6	−85.9	160.0	−160.0	−122.9	−97.6	−85.9	160.0	−160.0	−122.9	−97.6	−86.0	70.4	−127.2

	1,4-1,3-arm GlcNAcβ1,4-Manα1,3-Manβ-OR				*Chitotriose* GlcNAcβ1,4-GlcNAcβ1,4-G-lcNAc				
	Gnβ1,4-Mn		Mnα1,3-Mnβ		Gnβ1,4-Gn		Gnβ1,4-Gnβ		
Monomer	ϕ_1	ψ_1	ϕ_2	ψ_2	ϕ_1	ψ_1	ϕ_2	ψ_2	Nomenclature used for the dihedral angles
A	−63.1	100.5	65.9	−109.0	−79.2	99.1	−72.0	114.6	1,2 linkage: ϕ=O5–C1–O2–C2
B	−63.0	99.6	67.1	−103.6	−79.9	100.9	−70.5	113.7	ψ=C1–O2–C2–C1
C	−61.8	100.8	63.9	−127.3	−77.9	100.5	−73.4	110.6	1,3 linkage: ϕ=O5–C1–O3–C3
Average	−62.6	100.1	65.6	−113.3	−79.0	100.2	−72.0	113.0	ψ=C1–O3–C3–C2
S.D	0.7	0.6	1.6	12.4	1.0	0.9	1.5	2.1	1,4 linkage: ϕ=O5–C1–O4–C4
SWEET (model)	−75.6	122.8	70.4	−127.2	−75.6	124.3	−75.6	124.3	ψ=C1–O4–C4–C3
									1,6 linkage: ϕ=O5–C1–O6–C6
									ψ=C1–O6–C6–C5
									ω=O6–C6–C5–C4

Dihedral angles for the three molecules (A, B, C) in an asymmetric unit with average values and its standard deviation (S.D) are given. For comparison, the dihedral angles of unbound oligosaccharides generated from the SWEET Web-based program are given above. See the legend to Figure 5(a)–(c) for the detailed nomenclature of the dihedral angles. Gn, *N*-acetylglucosamine; Mn, mannose.

Table 4. Oligosaccharide–protein atom interactions
A. *Interactions with the oligosaccharides and the protein atoms (for comparison, chitobiose (CBO) interactions are taken from PDB: 1TW5)*

Ligand atoms	Protein atoms	Distance (Å)	Ligand atoms	Protein atoms	Distance (Å)
Pentasaccharide			*1,2-1,3-arm*		
Mid-Man			Mid-Man		
C1	282 Tyr CE2	3.68	O3	282 Tyr CE2	3.74
C6	356 Phe CE2	3.44	O5	356 Phe CE2	3.76
Pentasaccharide			*1,2-1,3-arm*		
Core-Man			Core-Man		
O6	282 Tyr CD2	3.87	O4	356 Phe CD2	3.66
O6	282 Tyr CE2	3.91	O4	356 Phe CE2	3.68
C5	282 Tyr CB	3.81	O4	359 Ile CD1	3.89
C5	282 Tyr CG	3.92	O6	356 Phe CD2	3.88
C6	282 Tyr CG	3.62	O6	359 Ile CD1	3.27
C6	282 Tyr CD2	3.49	*1,4-1,3-arm*		
C6	282 Tyr CE2	3.80	Mid-Man		
O5	282 Tyr CB	3.93	O6	282 Tyr CE2	3.99
O5	282 Tyr CD2	3.92	O6	282 Tyr CZ	3.95
O1	281 Pro O	3.60	*1,4-1,3-arm*		
C1	281 Pro O	3.92	Core-Man		
1,2-1,6-arm			O1	356 Phe CE1	3.72
Mid-Man			O1	356 Phe CE2	3.51
C1	282 Tyr CE2	3.72	O1	356 Phe CZ	3.08
C1	282 Tyr CZ	3.76	O2	356 Phe CZ	3.67
C1	282 Tyr OH	3.88	*Chitotriose*		
C2	282 Tyr CE2	3.97	Mid-GlcNAc		
C6	356 Phe CD2	3.81	O6	282 TYR CE2	3.95
C6	356 Phe CE2	3.50	O6	282 TYR CZ	3.74
C6	356 Phe CD2	3.94	O6	282 Tyr OH	3.94
1,2-1,6-arm			*Chitobiose*		
Core-Man			Reducing end		
O6	282 Tyr CD2	3.95	GlcNAc		
O6	282 Tyr CE2	3.85	C4	286 Tyr CE2	3.99
C5	282 Tyr CB	3.83	C6	286 Tyr CE2	3.91
C5	282 Tyr CG	3.72	C6	286 Tyr CZ	3.75
C5	282 Tyr CD1	3.86	C6	286 Tyr OH	3.84
C6	282 Tyr CG	3.83	O6	319 Asp OD2	3.91
C6	282 Tyr CD1	3.71			
C6	282 Tyr CE1	3.76			
C6	282 Tyr CD2	3.99			
C6	282 Tyr CZ	3.93			
O4	282 Tyr CD1	3.43			

B. *The number of interactions between the oligosaccharides and the protein atoms with corresponding apparent K_m*

	No. interactions			
Oligosaccahride	Mol A	Mol B	Mol C	Apparent K_m (mM)
Pentasaccharide	5	13	2	1.23(4)
GlcNAc β1,2-Manα1-6Manβ-OR	18	17	12	0.06(1)
GlcNAc β1,2-Manα1-3Manβ-OR	6	7	6	0.60(15)
GlcNAc β1,4-Manα1-3Manβ-OR	5	6	5	0.71(16)
Chitotriose	2	3	3	0.96(14)
Chitobiose[a]	5	2	–	1.59(32)

The maximum number of interactions between the ligand atoms (excluding the non-reducing end GlcNAc) and the protein atoms less than the 4.0 Å cutoff are given for the partially visible pentasaccharide and four different trisaccharides. Standard deviations are given in parentheses to their least significant decimal point.
[a] Interactions taken from PDB: 1TW5.

(±0.9)°) are different from one of the two distinct conformer values reported in the literature (ϕ = −80.1(±12.6)°, ψ = −97.6(±22.3)°),[16,17] whereas the ϕ, ψ values of Manα1,3-Man linkage (62.1(±1.3)°, −141.0(±4.4)°) match well with 130 out of 163 crystal structures (Table 3). The reducing end α1-3-mannose (core mannose) lies between Tyr282 and Phe356, making a few more interactions (<4.0 Å) with Phe356. There are fewer interactions between the 1,2-1,3-arm and the protein atoms than between the 1,2-1,6-arm and the protein atoms (Table 4A). The intersaccharide hydrogen bond is found between O3 of the middle mannose and O5 of the non-reducing end GlcNAc.

Structure of the complex with GlcNAcβ1,4-Manα1,3-Manβ-OR (1,4-1,3-arm) trisaccharide

The 1,4-1,3-arm trisaccharide unit is found in the antennae of the complex *N*-glycan structures (purple arrows shown in Figure 1). Since only a few crystal structures of the proteins with an oligosaccharide containing the GlcNAcβ1,4-Man

disaccharide unit are present in the PDB,[16,17] the dihedral angles observed in the present complex cannot be compared with those in the data base. On the other hand, the ϕ, ψ values of the Manα1,3-Man disaccharide unit represent a distinct conformation that matches with the literature values (Table 3).[16,17] Furthermore, the intersaccharide hydrogen bond between O3 of the middle mannose and O5 of the non-reducing end GlcNAc is also predominant in this complex. The reducing end mannose (α1,3-Man) is found more towards Phe356 than towards Tyr282 (Figure 3(d)) and makes few interactions with Phe356 (Table 4A).

Structure of the complex with GlcNAcβ1,4-GlcNAcβ1,4-GlcNAc (chitotriose) trisaccharide

Chitotriose is a linear molecule formed with β1,4 linkages and stabilized by intersaccharide hydrogen bonds between O3 of GlcNAc and O5 of the preceding GlcNAc residue. The dihedral angles (ϕ, ψ) of chitotriose, comprised of GlcNAcβ1,4-GlcNAc-linkages, agree well with the mean values (ϕ = −75.9(±11.6)° and ψ = 119.0(±15.4)°) observed in 376 out of 398 crystal structures,[16,17] and their angles are given in Table 3. Non-reducing end GlcNAc alone takes part in the formation of five conserved hydrogen bonds with the protein atoms, but the second (mid-GlcNAc) and the third GlcNAc residue from the non-reducing end do not involve hydrogen bonds. As chitotriose is a linear molecule (Figure 3(e)), the hydrophobic interactions with the protein atoms are very few for the mid-GlcNAc and completely absent for the third reducing end GlcNAc residue (Table 4A). A sulfate ion is found in the vicinity of chitotriose for a single molecule in the asymmetric unit.

Comparison of the structures of the oligosaccharides in complex with h-M340H-β4Gal-T1

An overall structural comparison of the bound trisaccharide 1,2-1,6-arm with the partial portion of visible pentasaccharide and modeled pentasaccharide (see Materials and Methods) is shown in Figure 4, and comparison with the 1,2-1,3-arm is shown in Figure 5(a). It is interesting to note that in the crystal structures the dihedral angles ϕ of the GlcNAcβ1,2-Man linkage in the trisaccharides 1,2-1,6-arm and 1,2-1,3-arm take similar values, whereas the ψ values are different (Table 3). After interacting with the protein atoms, the reducing end mannose (α1,6-Man or α1,3-Man) stabilizes the conformation of the trisaccharide, dictating a particular conformation for the dihedral angle ψ of the preceding β1,2-linkage in the respective trisaccharides. As a consequence, the rms deviation between the endocyclic atoms of the middle mannose of the 1,2-1,6-arm and the 1,2-1,3-arm trisaccharides, is large (1.76 Å), as observed by the superposition of the two bound trisaccharide (1,2-1,6-arm and 1,2-1,3-arm) structures (Figure 5(a)). Furthermore, the structural comparison of the partially visible bound pentasaccharide with the bound trisaccharides, 1,2-1,6-arm and 1,2-1,3-arm, shows that the middle mannose (second residue from the non-reducing end GlcNAc) deviates to a lesser extent (0.80 Å) when compared with the 1,2-1,6-arm than with the 1,2-1,3-arm (2.38 Å). This suggests that the 1,2-1,6-arm of the pentasaccharide is bound to h-M340H-β4Gal-T1.

Both 1,2-1,3-arm and 1,4-1,3-arm trisaccharides retain intersaccharide hydrogen interactions between O3 of the middle mannose and O5 of the non-reducing end GlcNAc, irrespective of the linkage between the two residues. A stereo view of the superimposed structures of two trisaccharides, 1,2-1,3-arm and 1,4-1,3-arm, is given in Figure 5(b). The ϕ, ψ values of the β1,4 linked disaccharide unit in the two bound trisaccharides, 1,4-1,3-arm and chitotriose, are very similar (Table 3; Figure 5(c)). The superposition of the two structures at the non-reducing end GlcNAc shows that the rms deviation between the endocyclic atoms of the middle mannose and middle GlcNAc is 0.49 Å. The Manα1,3-Man linkage of the 1,4-1,3-arm differs from the GlcNAcβ1,4-GlcNAc-linkage (at the reduc-

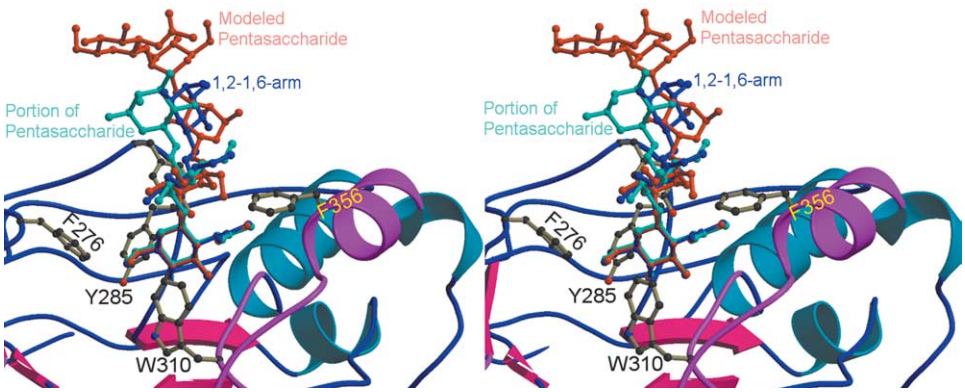

Figure 4. Stereo view of the modeled pentasaccharide (generated with the Web-based program SWEET) docked in the h-M340H-β4Gal-T1 that was in complex with the partially visible pentasaccharide. For comparison, the crystal structure-bound 1,2-1,6-arm trisaccharide (blue) and the visible partial portion of the pentasaccharide (cyan) is superimposed at the non-reducing end GlcNAc.

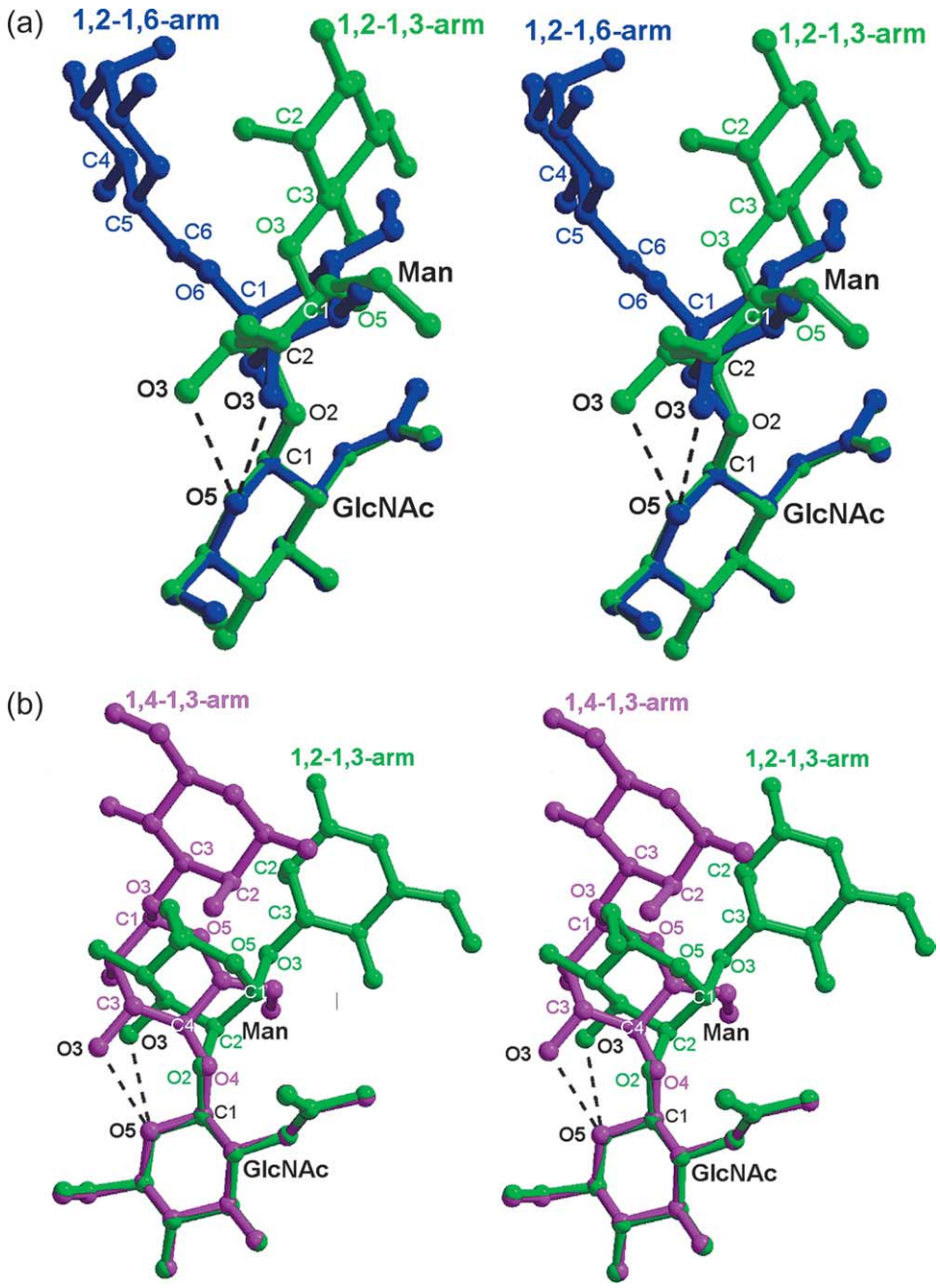

Figure 5 (*legend next page*)

ing end) of chitotriose, where core mannose of 1,4-1,3-arm interacts with protein, leading to lower K_m.

Implications of the oligosaccharide structures on the kinetic parameters

The true K_m for the monosaccharide GlcNAc is about 10 mM, which is six- to sevenfold higher, compared to the disaccharide chitobiose, GlcNAcβ1,4-GlcNAc (Table 1). The additional GlcNAc residue at the non-reducing end of chitobiose makes a few more molecular interactions in b-β4Gal-T1 (Table 4B) with the protein residue Y286, thus lowering its K_m (PDB code 1TW5).[14] In the case of chitotriose in complex with h-M340H-β4Gal-T1, the additional GlcNAc at the reducing end does not interact with the protein atoms, thus resulting in K_m for the trisaccharide chitotriose similar to that for the disaccharide chitobiose (Table 4B). In contrast, an extension in the disaccharide GlcNAcβ1,2-Man with one more monosaccharide residue to form trisaccharides (1,2-1,6-arm, 1,2-1,3-arm and 1,4-1,3-arm) lowers the apparent K_m for the trisaccharide compared to the disaccharide. The additional monosaccharide residue at the reducing end interacts with the protein atoms that contribute towards the lowering of apparent K_m (Table 4B).

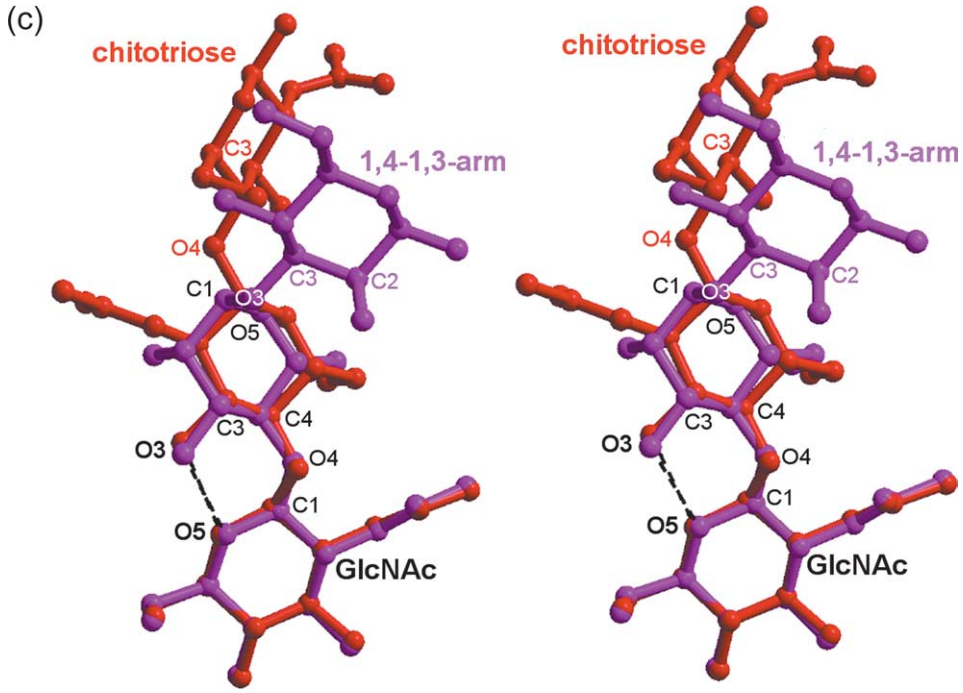

Figure 5. Stereo diagrams of superimposed trisaccharides bound to h-M340H-β4Gal-T1, illustrating the conformational differences between the trisaccharides. The atoms defining the dihedral angles (ϕ, ψ and ω) are labeled and color-coded according to the trisaccharide colors. The nomenclature of dihedral angles and values refer to Table 3. (a) Stereo view of two trisaccharides, 1,2-1,6-arm (blue) and 1,2-1,3-arm (green), bound to h-β4Gal-T1, superimposed at the non-reducing end GlcNAc, with GlcNAcβ1,2-Man as the common disaccharide unit. The hydrogen bond between O3 of the middle mannose and O5 of the non-reducing end GlcNAc is displayed for 1,2-1,6-arm and 1,2-1,3-arm. The nomenclature for the dihedral angles in 1,2-linkage is: ϕ = O5–C1 (GlcNAc)–O2–C2 (middle Man) and ψ = C1 (GlcNAc)–O2–C2–C1 (middle Man); 1,6-linkage is: ϕ = O5–C1 (middle Man)–O6–C6 (reducing end Man), ψ = C1 (middle Man)–O6–C6–C5 (reducing end Man) and ω = O6–C6–C5–C4 (reducing end Man); 1,3-linkage is: ϕ = O5–C1 (middle Man)–O3–C3 (reducing end Man) and ψ = C1 (middle Man)–O3–C3–C2 (reducing end Man). O5 of middle Man in 1,2-1,6-arm is buried and thus unlabeled. (b) Stereo view of two bound trisaccharides, 1,2-1,3-arm (green) and 1,4-1,3-arm (purple), superimposed at the non-reducing end GlcNAc with α1,3 linkage as the common linkage between the middle mannose and the reducing end mannose (core mannose). The hydrogen bond is found in both the 1,2-1,3-arm and the 1,4-1,3-arm, irrespective of the linkages between the non-reducing end GlcNAc and the middle mannose. The nomenclature for dihedral angles for 1,2-linkage is: ϕ = O5–C1 (GlcNAc)-O2–C2 (middle Man) and ψ = C1 (GlcNAc)–O2–C2–C1 (middle Man); 1,3-linkage is: ϕ = O5–C1 (middle Man)–O3–C3 (reducing end Man) and ψ = C1 (middle Man)–O3–C3–C2 (reducing end Man); 1,4-linkage is: ϕ = O5–C1 (GlcNAc)–O4–C4 (middle Man) and ψ = C1 (GlcNAc)–O4–C4–C3 (middle Man). (c) Stereo view of two bound trisaccharides, chitotriose (red) and 1,4-1,3-arm (purple), superimposed at the non-reducing end GlcNAc with β1,4 linkage as the common linkage between the non-reducing end GlcNAc and the middle saccharide. The hydrogen bond found in both chitotriose and the 1,4-1,3-arm between O3 of the middle sugar and O5 of non-reducing end GlcNAc is shown. The nomenclature for dihedral angles in the 1,4-linkage of chitotriose is: ϕ = O5–C1 (GlcNAc)–O4–C4 (succeeding GlcNAc) and ψ = C1 (GlcNAc)–O4–C4–C3 (succeeding GlcNAc); 1,4-linkage of 1,4-1,3-arm is: ϕ = O5–C1 (GlcNAc)–O4–C4 (middle Man) and ψ = C1 (GlcNAc)–O4–C4–C3 (middle Man); 1,3-linkage of 1,4-1,3-arm is: ϕ = O5–C1 (middle Man)–O3–C3 (reducing end Man) and ψ = C1 (middle Man)–O3–C3–C2 (reducing end Man). C4 of the reducing end GlcNAc in chitotriose is buried and thus unlabeled.

During remodeling of the *N*-glycan chains of glycoproteins in the Golgi apparatus, GlcNAc, Gal and sialic acid are added to the chains by corresponding GTs. At least seven *N*-acetylglucosaminyltransferase (GlcNAc-T) family members (I–VII) add GlcNAc sequentially to the branched antenna of *N*-glycans, and the branch specificity of these enzymes has been well established.[18] Pâquet *et al.*, using rat β4Gal-T, showed that the monogalactosylated biantennary *N*-glycan with GlcNAc on the 1,2-1,6-arm had higher affinity than the GlcNAc on the 1,2-1,3-arm.[19] However, the rate of galactose transfer to the GlcNAc on 1,2-1,3-arm was fivefold faster than to the GlcNAc on the 1,2-1,6-arm of the non-galactosylated biantennary *N*-glycan. Narasimhan *et al.*, using bovine milk β4Gal-T, showed that the ratio of the rates of galactosylation of the Manα1,3-arm to the Manα1,6-arm is 6.8 in the absence of bisecting GlcNAc, and 2.8 in the presence of bisecting GlcNAc.[20] Blanken *et al.*, using colostrum β4Gal-T, showed that the transfer of Gal to the β1,6 linked GlcNAc residue of a trisaccharide GlcNAcβ1,6-(GlcNAcβ1,3-)-Gal is 20 times faster than the transfer to the β1,3-linked GlcNAc residue.[21] These studies, however, did not determine which member of the β4Gal-T family was present in the enzyme preparations. Our findings are consistent with the above results, in

that the 1,2-1,6-arm trisaccharide has much lower apparent K_m for the T1 member of the human β4Gal-T family than the 1,2-1,3-arm trisaccharide. The structural investigations also reveal that, compared to other trisaccharides, the 1,2-1,6-arm, due to its greater conformational flexibility, makes the maximum number of interactions with the protein atoms of h-β4Gal-T1 (Table 4A). This correlates with its K_m, which is tenfold lower than that of the 1,2-1,3-arm and 1,4-1,3-arm trisaccharides, and 22-fold lower than that of chitotriose. The substrate inhibition at a lower concentration of the 1,2-1,6-arm trisaccharide compared to the 1,2-1,3-arm trisaccharide (Figure 2) is due to the higher affinity of the 1,2-1,6-arm trisaccharide towards β4Gal-T1, inducing the conformational change in the flexible loop of the enzyme, which closes the lid that covers the binding site before the donor substrate can bind to it.[4,9] The kinetic studies, together with the crystallographic studies, suggest that at a lower concentration, the 1,2-1,6-arm, rather than the 1,2-1,3-arm, of a biantennary *N*-glycan is the preferred antenna for galactosylation by β4Gal-T1, while at a higher concentration, the 1,2-1,3-arm is the preferred antenna. Other members of the β4Gal-T family may be preferentially transferring galactose to the 1,2-1,3-arm and acting in concert to galactosylate the various antennae of the *N*-glycans of glycoproteins.

Materials and Methods

Chitobiose (GlcNAcβ1,4-GlcNAc) and chitotriose (GlcNAcβ1,4-GlcNAcβ1,4-GlcNAc) were obtained from Sigma Chemicals, USA. The disaccharide GlcNAcβ1,2-Man and the pentasaccharide GlcNAcβ1,2-Manα1,6(GlcNAcβ1,2-Manα1,3)Man were purchased from Dextra-labs, UK. The heptasaccharide, Arg-[GlcNAcβ1,2-Manα1,6-(GlcNAcβ1,2-Manα1,3)-Manβ1,4-GlcNAcβ1,4-GlcNAcβ]-Asn-Glu-Gly, which carries both 1,2-1,6-arm and 1,2-1,3-arm linked to core mannose, was purchased from Calbiochem, USA.

The construction of the h-β4Gal-T1 and mutant h-M340H-β4Gal-T1 cDNA clones, protein expression in *Escherichia coli*, purification of the inclusion bodies, *in vitro* folding and purification of the folded h-M340H-β4Gal-T1 and h-β4Gal-T1, were carried out as described for b-β4Gal-T1.[14,22]

The protein sequence numbering of h-β4Gal-T1 is in accordance with the human β4Gal-T1 sequence deposited in the GenBank data base with accession number X13223.

The synthesis of trisaccharides

The three trisaccharides (1,2-1,6-arm, 1,2-1,3-arm and 1,4-1,3-arm) were synthesized using the previously established monosaccharide building blocks (see Supplementary Data), where the C3 and C6 positions of core β-mannose in trisaccharides were differentiated as described.[23–27] Assembly of fully protected trisaccharide precursors was achieved in reasonable yield. The final trisaccharides were obtained following global deprotection of the temporary protecting groups, and derivatization of the *N*-glycan moiety.[28] Each trisaccharide contains the linker sequence $–CH_2–CH_2–CH_2–CH=CH_2$, which is β-linked to the reducing end mannose. Concentrations of the synthetic trisaccharide solutions were determined using gas chromatography/mass spectrometry,[29] performed by Complex Carbohydrate Research Center, Athens, GA, USA. The commercial oligosaccharides used for kinetic studies were analyzed at NCI-Frederick using mass spectrometry.

Enzyme assay and determination of kinetic parameters

An *in vitro* assay procedure for h-β4Gal-T1 has been reported.[14] Kinetic parameters for UDP-Gal and either GlcNAcβ1-4GlcNAc (chitobiose) or GlcNAcβ1-4GlcNAcβ1-4GlcNAc (chitotriose) were determined using concentrations of UDP-Gal from 50–300 μM, and saccharide acceptor concentrations from 0–3 mM, and 5 mM Mn^{2+}.

The true K_m of the donor (K_A) and of the acceptor (K_B), and the turnover number (k_{cat}), were obtained using two-substrate analyses and the primary plots of at least five concentrations of donor (UDP-Gal) and six concentrations of acceptors, and the corresponding secondary plots of the intercepts and slopes. The data were analyzed for a general two-substrate system using the following equation[13,30] with EnzFitter, a non-linear curve-fitting program for Windows from Biosoft:

$$v = \frac{V_{max}[A][B]}{K_B[A] + K_A[B] + [A][B]}$$

The above rate equation is for the asymmetric initial velocity pattern associated with a sequential mechanism in which substrate A does not dissociate from the E.S complex. The kinetic parameters, K_A, i_B, and V_{max}, were obtained from the fitted curves. The data with the single donor substrate concentration were fit with the standard single-substrate Michaelis–Menten equation that gave apparent values of K_m for the acceptors, and V_m and k_{cat} of the reaction.

Crystallization and data collection of complexes of h-M340H-β4Gal-T1 and oligosaccharides (a pentasaccharide and four trisaccharides)

The h-M340H-β4Gal-T1 was co-crystallized with the heptasaccharide Arg-[GlcNAcβ1,2-Manα1,6-(GlcNAcβ1,2-Manα1,3)-Manβ1,4-GlcNAcβ1,4-GlcNAcβ]-Asn-Glu-Gly or the pentasaccharide GlcNAcβ1,2-Manα1,6(GlcNAcβ1,2-Manα1,3)Man; or trisaccharides GlcNAcβ1,2-Manα1,6-Manβ-OR (1,2-1,6-arm), or GlcNAcβ1,2-Manα1,3-Manβ-OR (1,2-1,3-arm), or GlcNAcβ1,4-Manα1,3-Manβ-OR (1,4-1,3-arm), or GlcNAcβ1,4-GlcNAcβ1,4-GlcNAc (chitotriose). All the oligosaccharide–M340H-β4Gal-T1 complexes were crystallized under identical conditions at room temperature using the hanging-drop, vapor-diffusion technique. A droplet of 2 μl of protein solution (20 mg/ml) containing oligosaccharide in 0.1 M Tris–HCl (pH 8.0), 25 mM UDP-H, 25 mM $MnCl_2$ was equilibrated against reservoir solution containing 0.1 M Mes (pH 6.5), 2% (v/v) dioxane, 1 M ammonium sulfate. The final concentrations of the oligosaccharides were: 1.25 mM pentasaccharide, 60 μM 1,2-1,6-arm, 60 μM 1,2-1,3-arm, 600 μM 1,4-1,3-arm, and 1.25 mM chitotriose.

Crystals grew to a maximum size in three days only in the presence of acceptor substrates (oligosaccharides). For data collection, crystals were transferred to mother liquor containing 20% (v/v) glycerol, and flash-frozen in liquid nitrogen. Data were collected using synchrotron radiation at the beam line X9B of the Brookhaven National Laboratory using a Quantum-4 CCD detector (oscillation of 0.5°,

exposure time of 30 s/frame). Data integration and reduction were performed using HKL-2000.[31] All complexes belong to the orthorhombic space group $C222_1$ possessing similar unit cell parameters ($a=107$ Å, $b=194$ Å, $c=143$ Å) with three molecules in the asymmetric unit. Except for the triantennary 1,4-1,3-arm complex (1.9 Å), all other complexes diffracted to a resolution of 2.0 Å.

Structure determination of complexes of h-M340H-β4Gal-T1 with oligosaccharides

Initially, the structure solution was carried out for a single complex (M340H-β4Gal-T1–UDP-H, Mn^{2+} and pentasacchride) by the molecular replacement method using the program suite AMoRe.[32,33] The catalytic domain of b-β4Gal-T1 was used as a search model, in which the sequence identity between the bovine and the human β4Gal-T1 is 89%. A good solution was obtained using the closed conformation of b-β4Gal-T1 without a substrate (PDB code 1O0R) as a starting model with a correlation coefficient of 0.78 and *R*-factor of 0.33. On successive rigid-body refinement and 100 cycles of positional minimization using CNS1.1,[34] with mlf target, the substrates (UDP-H and partial portion of pentasaccharide) and cofactor Mn^{2+} were identified using $(2F_o-F_c)$ and (F_o-F_c) maps. After careful inspection, the model was corrected using the graphics program O,[35] and then the substrates UDP-H and Mn^{2+} were fitted. Instead of pentasaccharide, only disaccharide was observed in two molecules, and in one molecule an extra electron density was observed. First, disaccharide (GlcNAcβ1,2-Man) was fit to three molecules in the asymmetric unit and refined. The coordinates of the disaccharide were generated using the Web-based program SWEET[36] and the CNS/O dictionary files were generated using XPLO2D.[37] Subsequent refinement revealed clear electron densities for the ordered solvent molecules, resulting in seven glycerol molecules, 14 sulfate ions, and one dioxane molecule. From difference Fourier maps at the 3σ level, 471 water molecules were located. Finally, the extended α1,6-linkage of the 1,2-1,6-arm in the pentasaccharide is visible with a low occupancy for the core mannose (70%) in one molecule. The trisaccharide unit GlcNAcβ1,2-Manα1,6-Man of the pentasaccharide was fit with the electron density for one molecule and disaccharide for the other two molecules. Bulk solvent corrections and overall anisotropic *B*-factor corrections were used throughout the refinement. Several cycles of positional and individual *B*-factor refinements were carried out until *R* and R_{free} converged. The refined structure was validated using PROCHECK.[32]

A similar procedure was used for the other four complexes, as all the complexes are isomorphous to each other. The detailed data collection and refinement statistics of all five data sets are summarized in Table 2. As we were able to see only the partial electron density for the pentasaccharide, we docked the modeled pentasaccharide generated from the SWEET Web-based program,[36] where the non-reducing end GlcNAc of the 1,2-1,6-arm was superimposed with the non-reducing end GlcNAc of partially visible pentasaccharide. The steric clash occurred when the 1,2-1,3-arm of the modeled pentasaccharide was superimposed with the non-reducing end GlcNAc of the partially visible pentasaccharide (not shown). Subsequently, the modeled pentasaccharide bound with β4-Gal-T1 was minimized by conjugate gradient method using SYBYL7.0. The linker sequence $-CH_2-CH_2-CH_2-CH=CH_2$, which is β-linked to the reducing end mannose, was not visible in the crystal structure of the complexes with the synthetic trisaccharides. Figures 3–5 were generated using the programs MOLSCRIPT[38] and Bobscript.[39] The superposition and rms deviations were calculated using the program ALIGN.[40]

Protein Data Bank accession numbers

Accession codes for the h-M340H-β4Gal-T1 crystal structure in complex with oligosaccharides in the PDB are 2AE7 (pentasaccharide), 2AEC (1,2-1,6-arm), 2AES (1,2-1,3-arm), 2AGD (1,4-1,3-arm) and 2AH9 (chitotriose).

Acknowledgements

The authors thank Dr Zbigniew Dauter (NSLS, X9B), and Mi Li (Macromolecular Crystallographic Laboratory) for their assistance in data collection, and Dr J. K. Mohana Rao for his valuable comments on the manuscript. The contents of this publication do not necessarily reflect the view or policies of the Department of Health and Human Services, nor does mention of trade names, commercial products or organization imply endorsement by the US Government. This project has been funded, in part, with the Federal funds from the NCI, NIH, under contract no. N01-C0-12400 and supported by the Intramural Research program of the NIH, National Cancer Institute, Center for Cancer Research.

Supplementary Data

Supplementary data associated with this article can be found, in the online version, at doi:10.1016/j.jmb.2005.07.050

References

1. Helenius, A. & Aebi, M. (2001). Intracellular functions of N-linked glycans. *Science*, **291**, 2364–2369.
2. Kornfield, R. & Kornfield, S. (1985). Assembly of asparagine-linked oligosaccharides. *Annu. Rev. Biochem.* **54**, 631–664.
3. Roseman, S. (2001). Reflections on glycobiology. *J. Biol. Chem.* **276**, 41527–41542.
4. Qasba, P. K., Ramakrishnan, B. & Boeggeman, E. (2005). Substrate-induced conformational changes in glycosyltransferases. *Trends Biochem. Sci.* **30**, 53–62.
5. Hennet, T. (2002). The galactosyltransferase family. *Cell. Mol. Life Sci.* **59**, 1081–1095.
6. Ramakrishnan, B., Balaji, P. V. & Qasba, P. K. (2002). Crystal structure of β1,4-Galactosyltransferase complex with UDP-Gal reveals an oligosaccharides acceptor binding site. *J. Mol. Biol.* **318**, 491–502.
7. Furukawa, K. & Okajima, T. (2002). Galactosyltransferase I is a gene responsible for progeroid variant of Ehlers-Danlos syndrome: molecular cloning and identification of mutations. *Biochim. Biophys. Acta*, **1573**, 377–381.
8. Paulson, J. C. & Colley, K. J. (1989). Glycosyltransferases. Structure, localization, and control of cell type-specific glycosylation. *J. Biol. Chem.* **264**, 17615–17618.
9. Ramakrishnan, B., Boeggeman, E., Ramasamy, V. &

Qasba, P. K. (2004). Structure and catalytic cycle of β-1, 4-galactosyltransferase. *Curr. Opin. Struct. Biol.* **14**, 593–600.
10. Gastinel, L. N., Cambillau, C. & Bourne, Y. (1999). Crystal structures of the bovine beta 1,4-galactosyltransferase catalytic domain and its complex with uridine diphosphogalactose. *EMBO. J.* **18**, 3546–3557.
11. Ramakrishnan, B. & Qasba, P. K. (2001). Crystal structure of lactose synthase reveals a large conformational change in its catalytic component, the beta 1, 4-galactosyltransferase-I. *J. Mol. Biol.* **310**, 205–218.
12. Ramakrishnan, B. & Qasba, P. K. (2003). Comparison of the closed conformation of the beta 1,4-galactosyltransferase-1 (beta 4Gal-T1) in the presence and absence of alpha-lactalbumin (LA). *J. Biomol. Struct. Dynam.* **21**, 1–8.
13. Boeggeman, E. & Qasba, P. K. (2002). Studies on the metal binding sites in the catalytic domain of β1,4-galactosyltransferase. *Glycobiology,* **12**, 395–407.
14. Ramakrishnan, B., Boeggeman, E. & Qasba, P. K. (2004). Effect of Met344His mutation on the conformational dynamics of bovine β1,4-galactosyltransferase: crystal structure of Met344His mutant in complex with chitobiose. *Biochemistry,* **43**, 12513–12522.
15. Rao, V. S. R., Qasba, P. K., Balaji, P. V. & Chandrasekaran, R. (1998). *Conformations of Carbohydrates*, Harwood Academic Publishers, The Netherlands.
16. Petrescu, A. J., Petrescu, S. M., Dwek, R. A. & Wormald, M. R. (1999). A statistical analysis of *N*- and *O*-glycan linkage conformations from crystallographic data. *Glycobiology,* **9**, 343–352.
17. Wormald, M. R., Petrescu, A. J., Pao, Y., Glithero, A., Elliott, T. & Dwek, R. A. (2002). Conformational studies of oligosaccharides and glycopeptides: complementarity of NMR, X-ray crystallography, and molecular modeling. *Chem. Rev.* **102**, 371–386.
18. Schachter, H. (1986). Biosynthetic controls that the branching and microheterogeneity of protein-bound oligosaccharides. *Biochem. Cell Biol.* **64**, 163–181.
19. Pâquet, M. R., Narasimhan, S., Schachter, H. & Moscarello, M. A. (1984). Branch specificity of purified rat liver Golgi UDP-galactose:*N*-acetylglucosamine β-1, 4-galactosyltransferase. *J. Biol. Chem.* **259**, 4716–4721.
20. Narasimhan, S., Freed, J. C. & Schachter, H. (1985). Control of glycoprotein synthesis. Bovine milk UDPgalactose:*N*-acetylglucosamine β-4-galactosyltransferase catalyzes the preferential transfer of galactose to the GlcNAcβ1,2Manβ1,3-branch of both bisected and nonbisected complex biantennary Asparagine-linked oligosaccharides. *Biochemistry,* **24**, 1694–1700.
21. Blanken, W. M., Hodghwinkel, G. J. M. & Van Den Eijnden, D. H. (1982). Biosynthesis of blood group I and i substances, specificity of bovine colostrum β-*N*-acetyl-D-glucosaminide β1→4galactosyltransferase. *Eur. J. Biochem.* **127**, 547–552.
22. Boeggman, E., Balaji, P. V., Sethi, N., Masibay, A. S. & Qasba, P. K. (1993). Expression and deletion constructs of bovine beta-1,4-galactosyltransferase in *Esherichia coli*: importance of Cys 134 for its activity. *Protein Eng.* **6**, 779–785.
23. Ratner, D. M., Plante, O. J. & Seeberger, P. H. (2002). A linear synthesis of branched high-mannose oligosaccharides from the HIV-1 viral surface envelope glycoprotein gp120. *Eur. J. Org. Chem.* **5**, 826–833.
24. Rademann, J., Geyer, A. & Schmidt, R. R. (1998). Solid-phase supported synthesis of the branched pentasaccharide moiety that occurs in most complex type *N*-glycan chains. *Angew. Chem. Int. Ed.* **37**, 1241–1245.
25. Hewitt, M. C. & Seeberger, P. H. (2001). Automated solid-phase synthesis of a branched *Leishmania* cap tetrasaccharide. *Org. Letters*, **3**, 3699–3702.
26. Blatter, G., Beau, J.-M. & Jacquinet, J.-C. (1994). The use of 2-deoxy-2 trichloroacetamido-D-glucopyranose derivatives in syntheses of oligosaccharides. *Carbohydr. Res.* **260**, 189–202.
27. Ziegler, T. (1994). Synthesis of the 5-aminopentyl glycoside of β-D-Gal*p*-(1→4)-β-D-Glc*p*NAc-(1→3)-L-Fucp and fragments thereof related to glycopeptides of human Christmas factor and the marine sponge *Microciona prolifera*. *Carbohydr. Res.* **262**, 195–212.
28. Ratner, D. M. (2004). Solution-phase and automated solid-phase synthesis of high-mannose oligosaccharides: application to carbohydrate microarray and biological studies. PhD thesis, Massachusetts Institute of Technology, Cambridge, MA.
29. York, W. S., Darvill, A. G., McNeil, M., Stevenson, T. T. & Albersheim, P. (1985). Isolation and characterization of plant cell walls and cell wall components. *Methods Enzymol.* **118**, 3–40.
30. Herbert, J. F. (1975). *Initial Rate Enzyme Kinetics*, Springer, New York.
31. Otwinowski, Z. & Minor, W. (1997). Processing of X-ray diffraction data collected in oscillation mode. *Methods Enzymol.* **276**, 307–326.
32. Collaborative Computational Project Number 4 (1994). The CCP4 suite: programs for protein crystallography. *Acta Crystallog. sect. D*, **50**, 760–763.
33. Navaza, J. (2001). Implementation of molecular replacement in AMoRe. *Acta Crystallog. sect. D*, **57**, 1367–1372.
34. Brünger, A. T., Adams, P. D., Core, G. M., DeLano, W. L., Gros, P., GrosseKunstleve, R. W. *et al*. (1998). Crystallography & NMR system: a new software suite for macromolecular structure determination. *Acta Crystallog. sect. D*, **54**, 905–921.
35. Jones, T. A., Zou, J. Y., Cowan, S. W. & Kjelgaard, M. (1991). Improved methods for building protein models in electron density maps and the location of errors in these models. *Acta Crystallog. sect. A*, **47**, 110–119.
36. Bohne, A., Lang, E. & von der Lieth, C. W. (1999). SWEET-WWW-based rapid 3D construction of oligo- and polysaccharides. *Bioinformatics*, **15**, 767–768.
37. Kleywegt, G. J. & Jones, T. A. (1997). Model-building and refinement practice. *Methods Enzymol.* **277**, 208–230.
38. Kraulis, P. J. (1991). MOLSCRIPT: a program to produce both detailed and schematic plots of structures. *J. Appl. Crystallog.* **24**, 946–950.
39. Esnouf, R. M. (1997). An extensively modified version of Molscript that includes greatly enhanced coloring capabilities. *J. Mol. Graph.* **15**, 132–134.
40. Cohen, G. E. (1997). ALIGN: a program to superimpose protein coordinates, accounting for insertions and deletions. *J. Appl. Crystallog.* **30**, 1160–1161.

Edited by R. Huber

(Received 2 May 2005; received in revised form 14 July 2005; accepted 19 July 2005)
Available online 8 August 2005